

The orphan G protein-coupled receptor, *Gpr161*, encodes the *vacuolated lens* locus and controls neurulation and lens development

Paul G. Matteson*, Jigar Desai*[†], Ron Korstanje[‡], Gloria Lazar*, Tanya E. Borsuk*, Jarod Rollins[‡], Sindhuja Kadambi*, Jamie Joseph*, Taslima Rahman*, Jason Wink*, Rym Benayed*, Beverly Paigen[‡], and James H. Millonig*^{§¶||}

*Center for Advanced Biotechnology and Medicine, [§]Department of Neuroscience and Cell Biology, University of Medicine and Dentistry of New Jersey–Robert Wood Johnson Medical School, Piscataway, NJ 08854; [‡]The Jackson Laboratory, Bar Harbor, ME 04609; and [¶]Department of Genetics, Rutgers University, Piscataway, NJ 08854

Edited by Kathryn V. Anderson, Sloan-Kettering Institute, New York, NY, and approved December 18, 2007 (received for review June 16, 2007)

The *vacuolated lens (vl)* mouse mutant causes congenital cataracts and neural tube defects (NTDs), with the NTDs being caused by abnormal neural fold apposition and fusion. Our positional cloning of *vl* indicates these phenotypes result from a deletion mutation in an uncharacterized orphan G protein-coupled receptor (GPCR), *Gpr161*. *Gpr161* displays restricted expression to the lateral neural folds, developing lens, retina, limb, and CNS. Characterization of the *vl* mutation indicates that C-terminal tail of *Gpr161* is truncated, leading to multiple effects on the protein, including reduced receptor-mediated endocytosis. We have also mapped three modifier quantitative trait loci (QTL) that affect the incidence of either the *vl* cataract or NTD phenotypes. Bioinformatic, sequence, genetic, and functional data have determined that *Foxe3*, a key regulator of lens development, is a gene responsible for the *vl* cataract-modifying phenotype. These studies have extended our understanding of the *vl* locus in three significant ways. One, the cloning of the *vl* locus has identified a previously uncharacterized GPCR-ligand pathway necessary for neural fold fusion and lens development, providing insight into the molecular regulation of these developmental processes. Two, our QTL analysis has established *vl* as a mouse model for studying the multigenic basis of NTDs and cataracts. Three, we have identified *Foxe3* as a genetic modifier that interacts with *Gpr161* to regulate lens development.

cataracts | *Foxe3* | spina bifida

Cataract and neural tube defects (NTDs) are two common human disorders. Both have a multifactorial basis with genetics and environment contributing to increased risk (1–3). Age-related cataract affects ≈20.5 million Americans over the age of 40, whereas cataract is the leading cause of childhood blindness worldwide (4, 5). NTDs affect the formation of the neural tube during neurulation and are the second most common human birth defect, occurring in ≈1/1,000 American Caucasian live births (1). Mouse mutants have been useful tools for studying human disease, but few of the >300 NTDs and cataract mutations model the multifactorial basis of these human diseases.

The *vacuolated lens (vl)* mutation arose spontaneously on the C3H/HeSnJ background, and *vl/vl* displays both congenital cataracts and NTDs. Vacuoles in the lens at birth have been described by Dickie (6), but no embryological assessment of the developing lens has been reported. Later studies discovered that *vl* mutant embryos exhibit two different neural tube phenotypes (7, 8). Approximately 50% of *vl/vl* embryos display lumbar-sacral spina bifida. In the other *vl/vl* embryos, the neural tube closes; however, dorsal phenotypes are observed, including a thinning of the midline neuroepithelium and epidermis, dilation of the dorsal ventricle, and the presence of ectopic neuroepithelial cells in the ventricle. All of these phenotypes have also been documented in a closed human NTD called embryonic hydromyelia (9). The *vl* mutation results in lethality in ≈50% of the *vl/vl*. The cause of the lethality is unknown, but because mouse NTD

mutants typically die before birth (10, 11), one likely possibility is the lumbar-sacral spina bifida. All surviving adult *vl/vl* mice display congenital cataracts and do not exhibit any obvious signs of spina bifida.

The neurulation phenotypes of *vl* embryos have been extensively studied by Wilson and Wyatt (7, 8, 12–14). Histological assessment of the dorsal midline phenotypes, ultrastructural EM studies of the neural folds, and cultures of mutant embryos indicate that the *vl* mutation affects the last step of neurulation, apposition, and fusion of the neural folds. The molecular regulation of neural fold fusion is not well understood. One reason is that mouse mutants defective at this last step of neurulation have been difficult to identify because unfused neural folds rapidly splay apart, which mimics defects in the elevation of the neural plate (10). Although there are >200 mouse mutants that affect neural tube closure (www.jax.org), *vl* is currently one of three mouse mutants considered to be defective in neural fold fusion (11). Thus the *vl* mutant provides a unique opportunity for studying this final stage of neurulation.

G protein-coupled receptors (GPCRs) constitute a large superfamily of proteins that are commonly used by cells to sense and respond to their environment. There are >360 nonsensory GPCRs in the human genome. The ligand for ≈200 of these receptors have been identified, whereas the remaining 160 receptors are orphan GPCRs because their endogenous ligands are not known (15). The binding of ligands to GPCRs activates cytoplasmic G proteins, allowing the receptors to transduce extracellular signals across the plasma membrane into the cell. These heterotrimeric G proteins then regulate the cellular response to the extracellular signal through numerous second-messenger cascades. Attenuation of GPCR signaling is also important and is achieved by phosphorylation of the receptor, which results in either a conformational change that affects G protein binding or reduced cell surface expression through receptor-mediated endocytosis (15, 16).

Author contributions: P.G.M., J.D., and R.K. contributed equally to this work; P.G.M., J.D., R.K., J.R., B.P., and J.H.M. designed research; P.G.M., J.D., R.K., G.L., T.E.B., S.K., J.J., J.W., and R.B. performed research; T.R. contributed new reagents/analytic tools; P.G.M., J.D., R.K., G.L., T.E.B., S.K., J.W., R.B., and J.H.M. analyzed data; and P.G.M., J.D., R.K., and J.H.M. wrote the paper.

The authors declare no conflict of interest.

This article is a PNAS Direct Submission.

Freely available online through the PNAS open access option.

Data deposition: The sequence reported in this paper has been deposited in the Genbank database (accession no. EF197953).

[†]Present address: Harvard Medical School and The Children's Hospital, 300 Longwood Avenue, Boston, MA 02115.

^{||}To whom correspondence should be sent. E-mail: millonig@cabm.rutgers.edu.

This article contains supporting information online at www.pnas.org/cgi/content/full/0705657105/DC1.

© 2008 by The National Academy of Sciences of the USA

Here, we report that the *vl* phenotypes are caused by a mutation in an orphan GPCR called *Gpr161*. We also describe *Gpr161* expression during early embryonic development, the effect of the *vl* mutation on *Gpr161* expression and subcellular localization, the mapping of three modifier loci that affect the penetrance of the *vl* NTD and cataract phenotypes, and the identification of *Foxe3* as a gene responsible for the *vl* cataract-modifying effect.

Results

Positional Cloning of the *vl* Locus. A single allele of the *vl* locus arose spontaneously on the C3H/HeSnJ background. In a previous C57BL/6J intercross the *vl* locus was mapped to a 5-cM region on distal mouse chromosome 1 (17). To fine-map the *vl* locus and identify the gene responsible for the *vl* phenotypes, we performed a MOLF/Ei intersubspecific intercross. A total of 854 F₂ mice were genotyped for simple sequence length polymorphism (SSLP) markers located in the *vl* region. Three informative recombinants of 193 F₂ *vl/vl* mice were identified, which localized the *vl* critical interval to a 0.96-Mb region between markers *D1Mit269* and *D1Mit539* (Fig. 1A). A separate CAST/Ei intercross with 58 *vl/vl* F₂ mice confirmed this map position.

Inspection of the mouse genome identified 11 transcripts, nine previously annotated genes and two spliced ESTs, in the *vl* critical region (Fig. 1A). The coding region of all 11 transcripts in the *vl* critical interval was sequenced from *+/+* C3H/HeSnJ and *vl/vl* DNA to identify mutations. An 8-bp exonic deletion was identified in *EST AY255596* in *vl/vl* but not *+/+* DNA (data not shown). PCR across the deletion generated a smaller amplicon, confirming the presence of the mutation (Fig. 1B). The 8-bp deletion was not observed in 19 additional inbred mouse strains, including all C3H substrains (see *Materials and Methods*), consistent with this deletion not being a polymorphism. Sequence and expression analysis of other transcripts in the *vl* critical interval did not identify any changes that were consistent with these genes encoding the *vl* locus (data not shown and see *Materials and Methods*). In addition, the 8-bp deletion segregated with the *vl* phenotypes in >1,000 meioses in *+/vl* × *+/vl* and *vl/vl* × *+/vl* matings in our C3H/HeSnJ colony, where no *+/+* or *+/vl* mice displayed a NTD or cataracts phenotype and all phenotypically mutant embryos and postnatal mice were homozygous for the deletion (data not shown). These genetic data provide evidence that the 8-bp deletion in *EST AY255596* is the mutation responsible for the *vl* phenotypes.

EST AY255596 is a partial EST that contains coding sequence for a putative orphan GPCR. Inspection of the mouse genome identified two sets of nonoverlapping ESTs (genome.ucsc.edu). RT-PCR using embryonic day (E) 8.5 cDNA and primers to the 5' portion and 3' portion of each set of ESTs generated a 1.9-kb product, which was then sequenced. Blastn and Blastp homology searches with our full-length mouse cDNA and predicted protein sequence demonstrated that the cloned gene was 87% and 92% identical on a nucleotide and amino acid level to a human orphan GPCR, *GPR161*. These results indicate that a previously uncharacterized orphan GPCR, *Gpr161*, is the gene responsible for the *vl* mutant phenotypes.

BLAT searches with the *Gpr161* cDNA sequence demonstrated the transcript is encoded by six exons (genome.ucsc.edu) (Fig. 1A). The predicted ORF is 1,587 nt or 529 aa in length with an estimated molecular mass of 58.5 kDa (ca.expasy.org). The *vl* mutation (8-bp deletion) is located in exon 4 of the transcript and is expected to cause a frameshift and premature stop codon 50 nt 3' of the deletion. The deletion in the incorporation of 16 novel amino acids (GAHGRRTVPGTQQQHR) and truncation of the GPCR at residue 386, deleting 143 (of 203) amino acids of the C-terminal tail (Fig. 1D). The mutant protein is predicted to be ≈15 kDa smaller than WT *Gpr161* (ca.expasy.org). Western analysis performed on lysates isolated from cells transfected

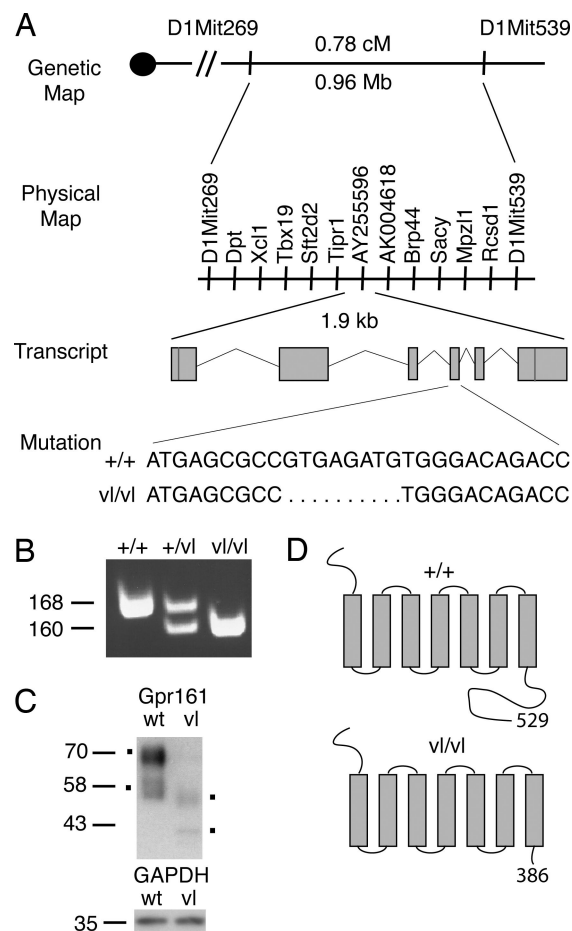


Fig. 1. Positional cloning of the *vl* mutation. (A) To clone the gene responsible for the *vl* mutation, MOLF/Ei and CAST/Ei intercrosses were performed. Recombinant mapping delimited the *vl* critical interval to 0.78 cM or 0.96 Mb. Genes within this interval are illustrated and were sequenced in *+/+* and *vl/vl* C3H/HeSnJ to identify the 8-bp deletion in exon 4 of *Gpr161*. The genomic structure of *Gpr161* transcript is depicted with red lines representing the position of start and stop codons. The nucleotide sequence surrounding the *vl* mutation is shown. (B) PCR across the deletion reveals a 160-bp amplicon in *vl/vl* compared with a 168-bp amplicon in *+/+* and both amplicons in *+/vl*. (C) Western analysis for N-terminal myc tagged WT and *vl*Gpr161 is shown and demonstrates the predicted smaller size for *vl*Gpr161. *vl*Gpr161 levels are also reduced compared with GAPDH. (D) Schematic representation of wt and *vl*Gpr161 protein with the predicted site of the C-terminal tail truncation illustrated.

with N-terminal myc-tagged WT and mutant (*vl*) *Gpr161* identified two major isoforms, with the smallest band migrating at the predicted size (≈58 kDa) and a larger band at ≈70 kDa (Fig. 1C). This larger band likely represents a modified version of *Gpr161* (ca.expasy.org; McVector version 9.0). The mutation reduces both protein products by ≈15 kDa, consistent with the mutation truncating the C-terminal tail. Reduced steady-state levels of the mutant isoforms were also observed (Fig. 1C).

***Gpr161* Expression Analysis.** We next investigated the developmental expression pattern of *Gpr161*. RT-PCR demonstrated that *Gpr161* was expressed from E8.5 to E11.5 [supporting information (SI) Fig. 5A]. *In situ* hybridization (ISH)-determined *Gpr161* expression was restricted to the lateral neural folds of the neural plate along the A-P axis (E8.0-E9.5) (Fig. 2A and B and SI Fig. 5B and C), consistent with *vl* affecting neural fold fusion (7, 8, 12–14). *Gpr161* is expressed at all examined stages of lens development: lens pit (E10.5), lens vesicle (E11.5), primary lens

Table 1. Summary of modifier loci for the *vl* mutation (Modvl)

Cross	QTL	Chromosome (cM)	Peak marker	LOD	95% C.I., cM	Phenotype	High allele	Mode of inheritance
B6	<i>Modvl1</i>	5 (44)	<i>D5Mit309</i>	3.7	38–50	Spina bifida	C3H	Dominant
CAST/Ei	<i>Modvl2</i>	1 (26)	<i>D1Mit236</i>	3.3	0–36	Spina bifida	C3H	Additive
MOLF/Ei	<i>Modvl3</i>	4 (51)	<i>D4Mit168</i>	4.2	45–61	Cataract	MOLF	Additive

chromosome 5 [44 cM, logarithm of odds (LOD) 3.7], and the allele effect at the peak marker, *D5Mit309*, demonstrated that the C3H background contributed to the spina bifida phenotype in a dominant fashion. For the CAST cross, when spina bifida was used as a covariate, *Modvl2* was mapped to chromosome 1 (26 cM, LOD 3.2). The C3H allele of *Modvl2* contributed to the spina bifida phenotype in an additive fashion (SI Fig. 9). *Modvl1* and *Modvl2* account for 15.9% and 13.1% of F₂ phenotypic variance in their respective crosses.

For the MOLF cross, a cataract modifier, *Modvl3*, was mapped to chromosome 4 (51 cM, LOD 4.2). Even though our *vl* MOLF intercross reduced the penetrance of cataract, the allele effect for *Modvl3* demonstrated that the MOLF background contributed to the cataract phenotype in an additive fashion. This finding is consistent with *Modvl3* and the *vl* mutation being responsible for cataracts on the mixed C3H/MOLF background. Other unidentified MOLF modifiers likely reduce the penetrance of the cataracts phenotype but these were not mapped because of their heterogeneity or low penetrance. *Modvl3* accounts for 9.9% of the F₂ phenotypic variance (SI Fig. 10). These data demonstrate that the penetrance of the *vl* spina bifida and cataract phenotypes are influenced by unlinked modifiers, establishing *vl* as a mouse model for studying the multigenic inheritance of these disease phenotypes.

Foxe3 and Modvl3 Cataract-Modifying Phenotype. To identify candidate genes that may contribute to the modifying effects of *Modvl1–3*, the 95% C.I. of *Modvl1–3* were scanned for biologically relevant candidates based on expression and disease phenotypes. This analysis identified *Foxe3* as a biologically relevant candidate for *Modvl3*. *Foxe3* is a winged helix forkhead transcription factor expressed in the developing lens and when mutated causes cataract and other lens-associated diseases in humans and mice. Knockdown of *Foxe3* in zebrafish also leads to a lens phenotype (21–25). *Foxe3*^{C3H} and *Foxe3*^{MOLF} were sequenced and two unique SNPs (mouse dbSNP build 127) were identified: a T-to-C transition at base pair 68 and an A-to-C transversion at base pair 499. The transversion does not result in an amino acid change, whereas the T^{C3H} to C^{MOLF} transition replaces a leucine (L^{C3H}) with a proline (P^{MOLF}) at amino acid 23 in the N terminus of the protein (Fig. 4A and data not shown).

This region of *Foxe3* was then sequenced in 22 other mouse strains. Eighteen of the strains had the A allele (L²³) at base pair 68, whereas only four had a C allele (P²³) (SI Fig. 11A). Although P²³ is not commonly observed in different mouse strains it is evolutionarily conserved in rat, cow, rhesus, chimp, and human (Fig. 4B). Given that proline commonly disrupts protein secondary structure, bioinformatics for *Foxe3*^{C3H} and *Foxe3*^{MOLF} were performed. For *Foxe3*^{C3H} a β -sheet is predicted to extend from amino acids 22–28 followed by an α -helix from amino acids 28–34. The P²³ substitution in *Foxe3*^{MOLF} shortens the β -sheet and inserts a turn at amino acid 28, preventing the formation of the α -helix (SI Fig. 11B). These bioinformatic data along with the evolutionary conservation of the proline suggest that the L²³ to P²³ alteration could functionally alter *Foxe3*.

If this amino acid change were responsible for the cataract-modifying effect, we would predict that genetic backgrounds with the L²³ allele would not affect the penetrance of the *vl* cataract phenotype. To investigate this possibility, a *vl* BALB/c

intercross was then performed. A total of 109 F₂ C3H/Balb progeny were generated (32 +/+, 63 +/vl, 13 vl/vl) with 100% of the *vl/vl* mice displaying an obvious cataract. These findings indicate that the BALB/c background does not modify the *vl* cataract phenotype, consistent with the P²³ allele in *Foxe3* contributing to the *Modvl3*-modifying effect.

We then investigated whether the L²³-to-P²³ alteration affects the activity of *Foxe3*. Because the N terminus of other forkhead transcription factors function as transactivators, *Foxe3*^{C3H} and *Foxe3*^{MOLF} were cotransfected with a luciferase (*luc*) construct driven by a consensus *Foxe3* binding site (26). To test the effect of the L²³-to-P²³ alteration, these constructs were transfected into HEK293T cells, which do not express endogenous *Foxe3* (data not shown and cgap.nci.nih.gov/SAGE). Both *Foxe3*^{C3H} and *Foxe3*^{MOLF} increased *luc* activity over the binding site alone. Moreover, *Foxe3*^{MOLF} resulted in significantly lower *luc* activity than *Foxe3*^{C3H}, indicating that the P²³ allele functionally alters the transcriptional activity of *Foxe3* (Fig. 4C). The lower activity of *Foxe3*^{MOLF} is also consistent with *Modvl3* enhancing the cataract phenotype. Thus, we provide sequence, protein mod-

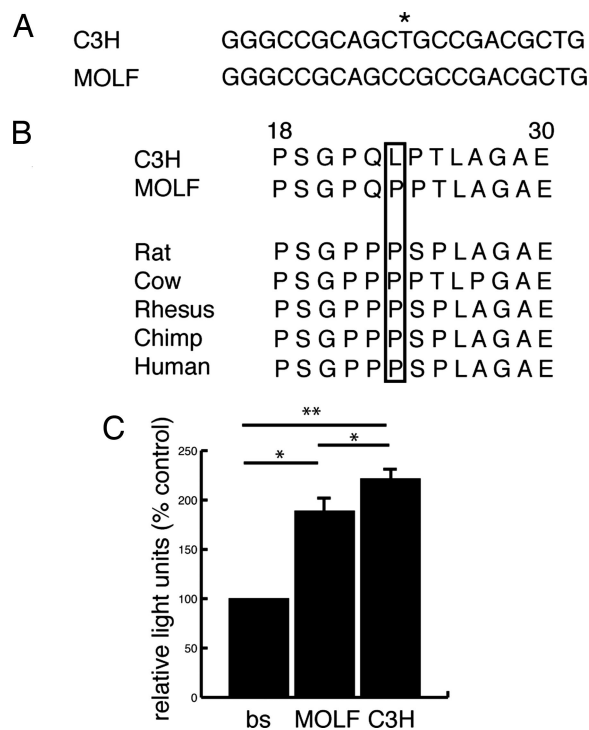


Fig. 4. *Foxe3*^{C3H} and *Foxe3*^{MOLF} allelic differences. (A) The T^{C3H}-to-C^{MOLF} SNP at base pair 68 (*) is shown with flanking sequence. (B) The T^{C3H}-to-C^{MOLF} transition replaces a leucine (L^{C3H}) with a proline (P^{MOLF}) at amino acid 23 in the N terminus of the protein. This amino acid change plus flanking amino acids (18–30 in mouse) is shown for C3H, MOLF, and other vertebrate species. The P²³ allele (boxed) is evolutionarily conserved from MOLF to humans. (C) Transient cotransfection assays revealed a functional difference in transcriptional activity between *Foxe3*^{C3H} and *Foxe3*^{MOLF}. Relative light units as percent control is shown for the *Foxe3* binding site-*luc* construct transfected individually (bs), with *Foxe3*^{MOLF} (MOLF) or *Foxe3*^{C3H} (C3H). *, *P* < 0.02; **, *P* < 0.007; one tailed paired Student's *t* test; *n* = 3.

eling, genetic, and functional data supporting *Foxe3* as a gene responsible for the cataract-modifying effect of *Modvl3*.

Discussion

Our positional cloning of the *vl* locus has identified *Gpr161*, an uncharacterized orphan GPCR, as one of the first genes necessary for neural fold apposition and fusion. We have also demonstrated that *Gpr161* is expressed in the lateral neural folds during neurulation and the *vl* mutation affects receptor-mediated endocytosis, a common mechanism used to attenuate GPCR signaling. These data suggest that Gpr161 signaling normally regulates downstream pathways necessary for neural fold apposition and fusion. This possibility is consistent with previous *vl* phenotypic analysis. Embryonic cultures of *vl* mutants demonstrated normal elevation and bending of the neural plate but apposition and fusion are abnormal (14), indicating that *vl* affects the pathways required for this last step of neurulation. In addition, EM studies in normal embryos have determined that cellular protrusions extend from the apical neural folds, which then interdigitate upon contact during neural fold fusion (27). In *vl* these cellular protrusions have an abnormal ultrastructural morphology (12). Future experiments should use *vl* to identify the molecular and cellular pathways regulated by Gpr161 during neural fold apposition and fusion.

It is well established that extracellular signals are essential for neurulation. Explant experiments have demonstrated that medial bending is induced by the notochord through Shh signaling (28) while the adjacent lateral surface ectoderm is required for elevation, dorso-lateral bending and formation and fusion of the neural folds. It has been suggested that the surface ectoderm like the notochord is a source of extrinsic factors important for neurulation (28, 29). Our results support this possibility and imply that a previously uncharacterized small molecule ligand is present in the neural environment, which binds and activates Gpr161 in the lateral neural folds during neurulation and is an important regulator of neural fold apposition and fusion.

Our ISH analysis has demonstrated that *Gpr161* is expressed at all stage of lens development. Interestingly, our phenotypic data has detected an obvious *vl* lens phenotype only after E14.5 (SI Fig. 12), suggesting that either this later stage is more sensitive to the *vl* mutation or subtle defects occur throughout lens development with a more severe phenotype being obvious only at later ages. The ocular environment is also known to contain secreted factors that regulate all stages of lens development. Although various secreted proteins (insulin-like growth factor 1, FGFs, Wnts, bone morphogenetic proteins) have been identified that coordinate these developmental processes (30), our results indicate that the small-molecule ligand for Gpr161 is another important regulator of lens development.

The *vl* mutation specifically deletes the C-terminal tail of Gpr161. Numerous mutagenesis studies have demonstrated that phosphorylation of serine and threonine residues in the C-terminal tail initiates receptor-mediated endocytosis (15, 16, 18, 19). Nine putative S/T phosphorylation sites are deleted by the *vl* mutation (ca.expasy.org; McVector version 9.0), consistent with our endocytosis phenotype. The C-terminal tail of GPCRs also serves as a scaffold for the binding of GPCR-interacting proteins (GIPs) that regulate receptor signaling (31). The *vl* mutation is likely to perturb the binding of these GIPs, which could affect additional aspects of Gpr161 activity. The mutation is then likely to have multiple effects on the Gpr161 protein including: reduced levels, decreased attenuation of receptor signaling, and altered binding of regulatory GIPs to the C-terminal tail. Together, these effects could lead to a complex Gpr161 signaling phenotype that may vary between cell types depending on the expression of different G proteins, kinases, and GIPs. In addition, the expression of *Gpr161* in *vl/vl* embryos and the targeting of the mutant receptor to the plasma membrane

indicate that *Gpr161^{vl}* is likely not a null allele. Conditional loss-of-function *Gpr161* alleles should be generated in the future to investigate whether *Gpr161* has additional functions during neurulation and lens development and other embryonic structures expressing *Gpr161*.

We have also demonstrated that genetic background significantly affects the penetrance of the *vl* cataracts and spina bifida phenotype, enabling us to map the position of three *vl* modifiers. In our crosses, $\approx 50\%$ of adult *vl/vl*-B6/C3H and CAST/C3H mice display a lumbar-sacral lesion and hind-limb paralysis, phenocopying important aspects of the human disorder and making it an valuable mouse model for studying the causes and effects of human spina bifida (20). It will be important in the future to examine the lumbar-sacral lesion in these mice to determine whether it has a similar or different neuropathology to what has been reported in humans and to investigate the cause of the hind-limb paralysis. The genetic loci responsible for this adult spina bifida phenotype have now been mapped to chromosome 5 (*Modvl1*-B6) and chromosome 1 (*Modvl2*-CAST/Ei). Because the B6 or CAST/Ei alleles of these QTL segregate with an absence of spina bifida, it will be interesting in future congenic experiments to determine whether these loci are sufficient to rescue the spina bifida phenotype.

One cataract-specific QTL, *Modvl3*, was mapped to chromosome 4 in our MOLF/Ei cross, and we have identified the lens transcription factor, *Foxe3*, as a gene that contributes to this modifying effect. In 2003 The Complex Trait Consortium established eight criteria for identifying modifier genes, requiring more than two to be fulfilled for positive identification (32). Our experiments fulfill four criteria: a previously unidentified coding polymorphism predicted to structurally alter the *Foxe3* protein; *Foxe3* expression in the lens, the structure affected by *Modvl3* (22); mutations or knockdown of *Foxe3* result in lens phenotypes in three different species (21, 23–26), and a functional difference in transcriptional activity between *Foxe3*^{C3H} and *Foxe3*^{MOLF} demonstrated by *in vitro* studies. The SNP also alters an evolutionarily conserved amino acid, consistent with the structural and functional differences observed between *Foxe3*^{C3H} and *Foxe3*^{MOLF}. Finally, crossing *vl* to BALB/c, a strain with the L²³ allele, did not affect the penetrance of cataract. These data provide considerable support for *Foxe3* as a gene responsible for the *Modvl3*-modifying effect. Consistent with this possibility *Foxe3* plays a central role in lens development, regulating numerous pathways including lens vesicle closure, proliferation of anterior epithelial cells, fiber cell differentiation, and α -crystallin transcription (22). Thus, reduced transcriptional activity of *Foxe3*^{MOLF} is likely to affect the expression of many downstream genes, which in combination with the Gpr161 *vl* mutation contributes to the cataract phenotype on the C3H/MOLF background. It remains possible that additional MOLF variants in the 95% C.I. for *Modvl3* also contribute to the cataract phenotype. To test whether the L²³-to-P²³ amino acid change is sufficient to enhance the *vl* cataract phenotype would require knock-ins not currently possible for the modifying strains. *Foxe3*^{MOLF} also likely interacts with unmapped MOLF modifiers that decrease cataract penetrance, adding another level of complexity that would not be recapitulated in the knock-in.

Because the phenotypic effect of *Modvl3* is observed only in the presence of the *vl* mutation and is not sufficient to cause cataract on a WT background, it is likely that *Foxe3* and Gpr161 function in the same or interacting pathways to regulate lens development. Coexpression of *Foxe3* and *Gpr161* in the same cell types during lens morphogenesis supports this possibility (E9.5–E10.5) (21, 23). Future experiments will help determine the functional relationship between *Foxe3* and Gpr161 by examining their expression in respective mouse mutants and the lens phenotype in compound mutants as well as determining whether Gpr161 functions upstream

or downstream of Foxe3 through a series of cell culture and *in vitro* experiments. Because these *vl* modifiers likely function in the same pathway as Gpr161, future analysis also should be directed at identifying genes for *Modv1* and 2. These genes likely function with Gpr161 to regulate the signaling pathways necessary for neural fold apposition and fusion and may also help identify the small-molecule ligand that binds and activates Gpr161 during neurulation and lens development.

Finally, *vl* provides an important resource for investigating the biological basis of human cataracts and NTDs. Several rare human disorders also have been reported to display both congenital cataracts and NTDs (33–35). *GPR161* is then an appropriate candidate for future mutational analysis for these disorders and human embryonic hydromyelia and congenital cataracts. This approach has been successful for congenital cataracts, where several genes that are mutated in the mouse are also affected in humans with the disease (*PAX6*, *PITX3*, *FOXE3*) (36). Given the modifiability of the mutant phenotypes, *vl* is also a useful mouse model for studying the more common forms of these diseases like lumbar-sacral spina bifida and age-related cataracts. Future association analysis can test whether *GPR161* and the *vl* modifiers are susceptibility loci, and together with the identification of the extracellular ligand for Gpr161, these studies may provide insight into the multifactorial basis of NTDs and cataracts.

Materials and Methods

Positional Cloning and Expression Analysis of Gpr161. The *vl* locus was mapped by intersubspecific intercrosses to MOLF/Ei and CAST/Ei. F₂ *vl/vl* were identified by mutant phenotype, and recombinants delimited the *vl* locus to a 0.96-Mb region. Eleven genes mapped to the *vl* minimal region, and each exon was sequenced, identifying the 8-bp deletion in *Gpr161*. Nineteen additional inbred strains were sequenced to investigate whether the deletion was a polymorphism. The 8-bp deletion was confirmed by PCR, which was subsequently used as a genotyping assay. Standard RT-PCR and ISHs were used to determine *Gpr161* expression in +/+ and *vl/vl* E8.0–E14.5 embryos.

Western Analysis and Immunocytochemistry. Full-length +/+ and *vl/vl* *Gpr161* was cloned 3' of an N-terminal myc epitope tag and transiently transfected

into HEK293T cells. Standard Western protocols were used with cMyc (1:1,000 dilution; Cell Signaling) and GAPDH (1:300 dilution; Chemicon) antibodies. For subcellular colocalization studies, the above constructs were transfected into HEK293T cells and after 18–20 h were fixed and immunostained by using standard protocols [primary antibody, cMyc (Cell Signaling); secondary antibody, Alexa-Fluor 568 (Molecular Probes)] under permeabilized (0.1% Triton X-100) and nonpermeabilized conditions. To further investigate the difference in subcellular localization, the constructs were cotransfected with GFP expression vectors targeted to the ER, plasma membrane, and nucleus (pEYFP-ER; pEYFP-Nuc; pEYFP-Mem; Clontech) followed by immunostaining [primary antibody, GFP (Molecular Probes); secondary antibody, Alexa-Fluor 488 (zcom-Molecular Probes)]. For endosome colocalization, standard protocols were followed (37); the HEK293T cells were serum starved for 2 h and then incubated with transferrin-Alexa-Fluor 488 (Molecular Probes) for 5 or 15 min before fixation and immunostaining.

QTL Analysis. Phenotypic and nonphenotypic F₂ *vl/vl* B6, CAST, and MOLF/C3H mice were used for QTL analysis. These mice were identified by their C3H/C3H genotype for multiple chromosome 1 microsatellite markers flanking the *vl* locus (see *SI Text*). For the B6 and CAST crosses, the spina bifida, but not the cataract, phenotype was recorded, whereas for the MOLF cross all phenotypes were recorded. A total of 86–132 F₂ *vl/vl* depending on cross were genotyped for 60–80 SSLP markers evenly spaced throughout the genome. QTL analysis was performed as described (38).

Foxe3 Analysis. OMIM and expression databases (genome.ucsc.edu) identified *Foxe3* as a candidate gene. Sequence analysis was performed as described above. Bioinformatic evolutionary analysis and protein modeling was performed with McVector version 9.0, with the later using both Robson-Garnier (*SI Fig. 11B*) and Chou-Fasman algorithms. The *vl* BALB/c intercross was performed as described above, and cataract was noted by an obvious opacity of the lens. To test for a functional difference between Foxe3^{C3H} and Foxe3^{MOLF}, both versions of the gene were cloned into the BamHI site of pCMV-Tag3 expression vector after PCR amplification and sequence verification. HEK293T cells were transfected with 1.6 μg of the luc reporter, *Foxe3* expression constructs, and 10 ng of phRL-null vector by using Lipofectamine 2000. Twenty-four hours after transfection, standard protocols for calculating normalized luciferase values were conducted.

See *SI Text* for more details.

ACKNOWLEDGMENTS. We thank Theolyn Gilley for technical support. This work was supported by New Jersey Commission on Spinal Cord Research Grants 02-3016-SCR-5-0 and 04-2901-SCR-E-0 (to J.H.M.).

1. Detrait ER, George TM, Etchevers HC, Gilbert JR, Vekemans M, Speer MC (2005) *Neurotoxicol Teratol* 27:515–524.
2. Hammond CJ, Duncan DD, Snieder H, de Lange M, West SK, Spector TD, Gilbert CE (2001) *Invest Ophthalmol Visual Sci* 42:601–605.
3. Hammond CJ, Snieder H, Spector TD, Gilbert CE (2000) *N Engl J Med* 342:1786–1790.
4. Congdon N, Vingerling JR, Klein BE, West S, Friedman DS, Kempen J, O'Colmain B, Wu SY, Taylor HR (2004) *Arch Ophthalmol* 122:487–494.
5. Ezegwui IR, Umeh RE, Ezepeue UF (2003) *Br J Ophthalmol* 87:20–23.
6. Dickie M (1967) *Mouse News Lett* 36:39–40.
7. Wilson DB, Wyatt DP (1986) *J Neuropathol Exp Neurol* 45:43–55.
8. Wilson DB, Wyatt DP (1988) *Anat Embryol* 178:559–563.
9. Ikenouchi J, Uwabe C, Nakatsu T, Hirose M, Shiota K (2002) *Acta Neuropathol* 103:248–254.
10. Juriloff DM, Harris MJ (2000) *Hum Mol Genet* 9:993–1000.
11. Copp AJ, Greene ND, Murdoch JN (2003) *Nat Rev Genet* 4:784–793.
12. Wilson DB, Wyatt DP (1989) *Acta Neuropathol* 79:94–100.
13. Wilson DB, Wyatt DP (1992) *Teratology* 45:105–112.
14. Wilson DB, Wyatt DP (1993) *J Neuropathol Exp Neurol* 52:253–259.
15. Gainetdinov RR, Premont RT, Bohn LM, Lefkowitz RJ, Caron MG (2004) *Annu Rev Neurosci* 27:107–144.
16. Prossnitz ER (2004) *Life Sci* 75:893–899.
17. Mu J, Gilley T, Turner R, Paigen B (1996) *Mamm Genome* 7:770.
18. Koch T, Schulz S, Schroder H, Wolf R, Raulf E, Holt V (1998) *J Biol Chem* 273:13652–13657.
19. Roth A, Kreienkamp HJ, Nehring RB, Roosterman D, Meyerhof W, Richter D (1997) *DNA Cell Biol* 16:111–119.
20. Volpe J (1995) *Neurology of the Newborn* (Saunders, Philadelphia), 3rd Ed, pp 5–21.
21. Blixt A, Mahlapuu M, Aitola M, Pelto-Huikko M, Enerback S, Carlsson P (2000) *Genes Dev* 14:245–254.
22. Medina-Martinez O, Jamrich M (2007) *Development* 134:1455–1463.
23. Brownell I, Dirksen M, Jamrich M (2000) *Genesis* 27:81–93.
24. Semina EV, Brownell I, Mintz-Hittner HA, Murray JC, Jamrich M (2001) *Hum Mol Genet* 10:231–236.
25. Valleix S, Niel F, Nedelec B, Algros MP, Schwarz C, Delbos B, Delpech M, Kantelip B (2006) *Am J Hum Genet* 79:358–364.
26. Ormestad M, Blixt A, Churchill A, Martinsson T, Enerback S, Carlsson P (2002) *Invest Ophthalmol Visual Sci* 43:1350–1357.
27. Geelen JA, Langman J (1979) *Anat Embryol* 156:73–88.
28. Ybot-Gonzalez P, Cogran P, Gerrelli D, Copp AJ (2002) *Development* 129:2507–2517.
29. Moury JD, Jacobson AG (1989) *Dev Biol* 133:44–57.
30. Lovicu FJ, McAvoy JW (2005) *Dev Biol* 280:1–14.
31. Bockaert J, Fagni L, Dumuis A, Marin P (2004) *Pharmacol Ther* 103:203–221.
32. Abiola O, Angel JM, Avner P, Bachmanov AA, Belknap JK, Bennett B, Blankenhorn EP, Blizard DA, Bolivar V, Brockmann GA, et al. (2003) *Nat Rev* 4:911–916.
33. Dobyns WB, Pagon RA, Armstrong D, Curry CJ, Greenberg F, Grix A, Holmes LB, Laxova R, Michels VV, Robinow M, et al. (1989) *Am J Med Genet* 32:195–210.
34. Siegel-Bartlett J, Levin A, Teebi AS, Kennedy SJ (2002) *J Med Genet* 39:145–148.
35. Sniderman LC, Koenekoop RK, O'Gorman AM, Usher RH, Sufrategui MR, Moroz B, Watters GV, Der Kaloustian VM (2000) *Am J Med Genet* 90:146–149.
36. Graw J (2004) *Int J Dev Biol* 48:1031–1044.
37. Murph MM, Scaccia LA, Volpicelli LA, Radhakrishna H (2003) *J Cell Sci* 116:1969–1980.
38. Sugiyama F, Churchill GA, Higgins DC, Johns C, Makaritsis KP, Gavras H, Paigen B (2001) *Genomics* 71:70–77.